Fano Signatures in the Intersubband Terahertz Response of Optically Excited Semiconductor Quantum Wells

D. Golde,[1,*] M. Wagner,[2] D. Stehr,[2] H. Schneider,[2] M. Helm,[2] A. M. Andrews,[3] T. Roch,[3] G. Strasser,[3] M. Kira,[1] and S. W. Koch[1]

[1]*Department of Physics and Materials Sciences Center, Philipps-University, Renthof 5, 35032 Marburg, Germany*
[2]*Institute of Ion Beam Physics and Materials Research, Forschungszentrum Dresden-Rossendorf, P.O. Box 510119, 01314 Dresden, Germany*
[3]*Solid State Electronics Institute, Micro- & Nanostructure Center, TU Wien, Floragasse 7, 1040 Vienna, Austria*

(Received 12 December 2008; published 24 March 2009)

Absorption and transmission spectra of broadband terahertz pulses are measured to probe the intersubband response of an optically excited quantum-well heterostructure. While the terahertz absorption shows the single peak of the resonant intersubband transition, the transmission spectra display strong Fano signatures due to the phase sensitive superposition of ponderomotive and terahertz currents as predicted by our microscopic theory.

DOI: 10.1103/PhysRevLett.102.127403 PACS numbers: 78.67.De, 42.25.Bs, 73.21.Fg

Terahertz (THz) experiments on optically excited or doped semiconductors provide unique opportunities to analyze and manipulate low-energy excitations or quasiparticle states, like intersubband transitions between quantum confined states [1–5], excitons, or plasmons, and monitor their dynamical evolution [6–10]. With sufficiently strong THz pulses, one can even reach the regime of ''extreme nonlinear optics'' leading to effects such as Rabi flopping [5,11,12], ac-Stark splitting [13], or the dynamical Franz-Keldysh effect [14,15]. The microscopic analysis of these experiments shows that the THz wave propagating through the semiconductor is determined by the combined response of the so-called ponderomotive current and the true THz transitions. Here, the ponderomotive contribution refers to the charge current generated by the classical field that causes a wiggling motion of the carriers according to the acceleration theorem $\hbar\dot{\mathbf{k}} = -e\mathbf{E}_{\mathrm{THz}}$ [16,17]. This part of the light-matter interaction, often thought to be relevant only at high intensities [15], produces the simple response $\chi(\omega) = -\frac{\omega_{\mathrm{PL}}^2}{\omega^2}$ with the plasma frequency ω_{PL}. Because of the factor ω^{-2}, the ponderomotive contribution can usually be neglected in the analysis of interband optical excitation; however, it is of relevance in the THz regime even at the lowest intensities. Thus, the THz response of an excited semiconductor is influenced by ponderomotive effects plus the true THz transitions. When both contributions are of equal strength, one expects a strong interplay. In the experiments reported in Refs. [12,18] the evidences for the role of the ponderomotive current are rather indirect. Their influence could only be seen by virtue of a theoretical switch-off analysis.

To clearly expose the interplay of ponderomotive and true THz response, one needs an experimental method that makes it possible to observe both effects directly. In this Letter, we study the intersubband transition of photoexcited semiconductor quantum wells using linear THz spectroscopy. Monitoring the transmission of a broadband THz pulse, we directly observe signatures of the ponderomotive motion of the excited carriers. We show that interference of ponderomotive and resonant contributions produces a characteristic Fano-like line shape in the differential transmission spectrum.

Asymmetric Fano line shapes are known to result from quantum interference of discrete energy levels coupled to a nearby continuum [19] and have been observed in semiconductor heterostructures under various conditions [20–23]. Whereas the relevant continuum in typical Fano configurations is an integral part of the probed quantum object, in our system an effective continuum is provided by the light-matter interaction through the ponderomotive contribution.

Figure 1(a) shows the basic concept of our experiment where spectrally broadband THz pulses probe the sample's intersubband transition after resonant photoexcitation. The THz pulses are generated in a 55 μm thin z-cut GaSe crystal by phase-matched difference frequency mixing [24] within the broad spectrum of 12 fs optical pulses, delivered by a 78 MHz Ti:sapphire oscillator (Femtolasers: Femtosource Scientific sPro). The THz beam is focused by off-axis parabolic mirrors on the multi-quantum-well (MQW) sample, with the THz field having a strong component perpendicular to the MQW plane to couple effectively to the intersubband transition [25]. For THz-field-resolved detection, phase-matched electro-optic sampling [26,27] is applied. To this end, a weak component of the 12 fs laser beam goes through a delay stage and samples the THz-field induced polarization change in a second 30 μm thin z-cut GaSe crystal as a function of the time delay between THz pulse and sampling pulse [Fig. 1(c)].

The sample studied consists of 60 periods of 8.2-nm-thick undoped GaAs quantum wells, separated by 19.6-nm-thick barriers of $Al_{0.34}Ga_{0.66}As$. The sample was prepared

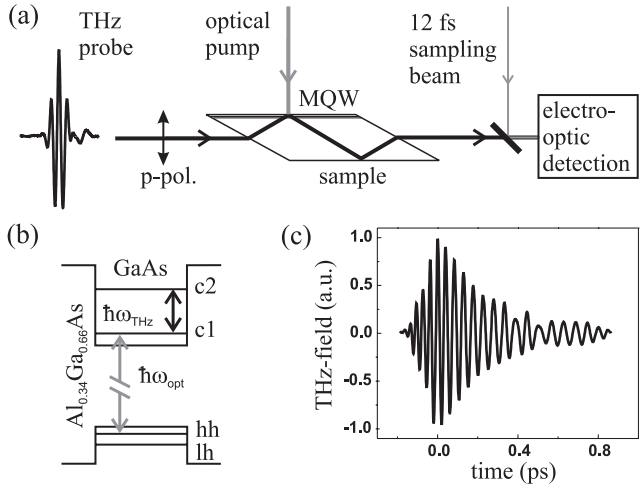

FIG. 1. (a) Optical interband pump intersubband THz probe experiment. (b) The transition from the heavy-hole (hh) state to the first conduction state (c1) in the $Al_{0.34}Ga_{0.66}As/GaAs$ multi-quantum-well (MQW) sample is resonantly excited, either by a ps or a fs laser. THz pulses probe the c1-to-c2 transition 25 ps after photoexcitation. (c) The field transients of the transmitted THz pulses are detected by phase-matched electro-optic sampling with a sampling beam. The reference without photoexcitation is shown.

in a 38-degree wedged-waveguide geometry, as shown in Fig. 1(a). To ensure optimized overlap between MQW region and THz standing wave [25], an additional $Al_{0.34}Ga_{0.66}As$ spacer layer of 300 nm thickness was grown on top of the sample. The experiments are performed at a temperature of 6 K.

The photoexcitation scheme is illustrated in Fig. 1(b). An optical interband pump pulse excites the MQW resonantly at the 1s heavy-hole exciton and creates carriers in the first conduction band. We choose either spectrally narrow 2.5 ps or broadband 100 fs optical excitation centered at $\hbar\omega_{opt} = 1.56$ eV. Both lasers are 78 MHz Ti:sapphire oscillators (Spectra Physics: Tsunami), locked to the repetition rate of the THz generating laser. In each case, only the first conduction subband of the MQW is populated. After a time delay of 25 ps during which the optically induced interband coherences disappear, the weak broadband THz-pulse probes the c1-to-c2 intersubband transition. In all the experiments, the photoexcited carrier density is 2×10^{10} cm^{-2} per quantum well.

A two-lock-in technique is employed to measure the transmitted THz transients with and without excitation. The visible pump and THz probe beams are chopped simultaneously at different frequencies around 2 kHz. The first lock-in amplifier locks on the modulation of the optical pump beam. Since the THz beam is also chopped at the same time, twice the signal obtained by the first lock-in amplifier yields the differential transmission $\Delta E(t)$, i.e., the pump-induced change in the transmitted THz field. The second lock-in amplifier detects the mean value between transmission with and without photoexcitation, leading to the reference $E_{ref}(t)$ without excitation by subtracting the signal of the first lock-in amplifier. This allows us to record $\Delta E(t)$ and $E_{ref}(t)$ simultaneously under the same conditions, preventing a drift in the relative phase between them. Such a phase drift would strongly affect the computed total THz absorption of the quantum wells $\alpha(\omega)$, where the complex valued Fourier transforms of $\Delta E(t)$ and $E_{ref}(t)$ enter in the following way: $\alpha(\omega) = 2\mathrm{Im}[-i\Delta E(\omega)/E_{ref}(\omega)]$. This relation follows from Maxwell's equations and the assumptions that (i) $|\Delta E| \ll |E_{ref}|$, (ii) the unexcited sample is nonabsorptive in the investigated frequency range, and (iii) only the single-pass signal is measured.

Figure 1(c) shows the reference transient $E_{ref}(t)$. Compared with the incident THz transient [Fig. 1(a)], the field oscillations last longer in time due to dispersion in the sample. The differential THz transmission transients $\Delta E(t)$ are presented in Figs. 2(a) and 2(b) for ps and fs excitation, respectively. First, one observes that the signal has 440 fs

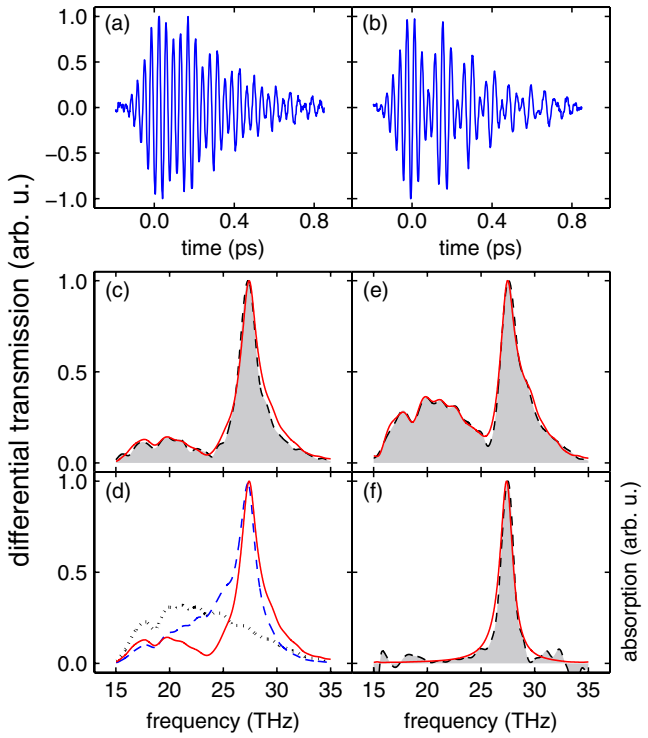

FIG. 2 (color online). Experiment-theory comparison of the THz intersubband response. (a),(b) Measured time-resolved differential transmission signals $\Delta E(t)$ for ps and fs excitation, respectively. (c) Measured spectral amplitude of differential transmission $|\Delta E(\omega)|$ (shaded area) and calculated current density $|J_{tot}(\omega)|$ (red solid line) after optical ps excitation. (d) shows the decomposition of the computed total current density (red solid line) into the ponderomotive contribution $|J_A|$ (black dotted line) and the intersubband current $|J_{THz}|$ (blue dashed line). (e), (f) Measured (shaded area) and computed (red solid line) differential transmission and THz absorption, respectively, after fs excitation. Here, J_A has been enhanced by 1.85 in order to account for substrate excitations.

decay constant for both ps and fs excitation, whereas a decay of 240 fs is observed for the reference $E_{\mathrm{ref}}(t)$ [see Fig. 1(c)]. This reveals the dephasing of the reradiated THz-induced intersubband polarization [2,3,28]. Second and more interesting, one observes a clear beating compared to the reference $E_{\mathrm{ref}}(t)$, superimposed on the dephasing and being more pronounced for fs photoexcitation.

We first address the ps excitation to analyze the origin of the observed beating. Figure 2(c) shows the spectral amplitude of the measured differential THz transmission $|\Delta E(\omega)|$ after optical excitation at the $1s$ position of the heavy-hole exciton resonance. We see that the spectrum consists of two major contributions: (i) a sharp resonance peak at the transition frequency of the conduction subbands $\nu_{1,2} = 27.3$ THz and (ii) a broad contribution centered at roughly 20 THz, being responsible for the beating in the time domain. These features remind us of a typical Fano spectrum, i.e., an undershoot at the low-frequency side of the peak followed by an asymmetric line shape.

When the system is excited with a 100 fs pulse, the broad contribution and the Fano signatures are more pronounced than in the ps case [Fig. 2(e)]. To check whether the broad feature in the differential transmission is caused by an additional carrier transition besides the intersubband resonance, we measure the THz absorption. Figure 2(f) shows that the absorption is single peaked; i.e., only the intersubband resonance appears and no Fano-like signature is observed.

In order to explain the experimental findings, we compute the THz transmission of a quantum well positioned at $z = 0$ (where z is the growth direction of the quantum well). The THz response follows from the wave equation

$$\left(\nabla^2 - \frac{n_b^2}{c^2}\frac{\partial^2}{\partial t^2}\right)E(\mathbf{r}, t) = \mu_0 \delta(z)\frac{\partial}{\partial t}(J_{\mathrm{A}}(t) + J_{\mathrm{THz}}(t)), \quad (1)$$

where n_b is the background refractive index, c is the speed of light, and μ_0 is the permeability of free space. The delta function arises due to the fact that the quantum-well width is much smaller than the wavelength of the THz field. The induced current density appearing as source term on the right-hand side of Eq. (1) consists of two terms: J_{THz} is the current due to the intersubband transitions and J_{A} describes the ponderomotive motion of the excited carriers due to the THz field. Solving Eq. (1), one finds that the differential transmission, i.e., the field that is reemitted by the current density, is directly proportional to the induced current [29]: $\Delta E \propto J_{\mathrm{A}} + J_{\mathrm{THz}}$.

The ponderomotive contribution to the current density is given by $J_{\mathrm{A}} = -\sum_\lambda \frac{e^2 n_\lambda}{m_\lambda} A_{\mathrm{THz}}$ [30] where n_λ is the carrier density in band λ and m_λ is the effective mass. The vector potential A_{THz} of the THz pulse is defined via $E_{\mathrm{THz}} = -\frac{\partial}{\partial t}A_{\mathrm{THz}}$. Here, λ includes both bulk-band index and subband index. Obviously, the ponderomotive current directly follows A_{THz} with an opposite phase due to the minus sign in J_{A}. The linear susceptibility $\chi_{\mathrm{A}}(\omega) = -\frac{\omega_{\mathrm{PL}}^2}{\omega^2}$ following from the ponderomotive current is a real-valued quantity. Consequently, J_{A} does not contribute to the absorption $\alpha(\omega) \propto \omega \mathrm{Im}[\chi(\omega)]$, but simply introduces a refractive index change to the excited material.

The THz current is computed via $J_{\mathrm{THz}} = \frac{1}{S}\sum_{\lambda,l,l',\mathbf{k}} j^\lambda_{l',l} p^\lambda_{l,l',\mathbf{k}}$ with the quantization area S and the matrix elements $j^\lambda_{l,l'}$. The quantity $p^\lambda_{l,l',\mathbf{k}}$ represents the microscopic intersubband polarization between subbands l and l' of bulk-band λ. The intersubband matrix element is given by $j^\lambda_{l,l'} = -\frac{i\hbar e}{m_\lambda}\int dz \xi^*_{\lambda,l}(z)\frac{\partial}{\partial z}\xi_{\lambda,l'}(z)$ where $\xi_{\lambda,l}(z)$ is the confinement wave function of the carriers.

The intersubband polarization $p^\lambda_{l,l',\mathbf{k}}$ in J_{THz} is computed microscopically with an equation-of-motion approach. Since we are interested only in the c1-to-c2 transition, we can restrict the sum to $\lambda = c$ and $l, l' \in \{1, 2\}$. In analogy to the semiconductor Bloch equations [31], one finds for the time evolution of the intersubband polarization

$$\begin{aligned} i\hbar\frac{\partial}{\partial t}p^c_{1,2,\mathbf{k}} = {} & (\tilde{\varepsilon}^c_{2,\mathbf{k}} - \tilde{\varepsilon}^c_{1,\mathbf{k}})p^c_{1,2,\mathbf{k}} + \frac{\partial}{\partial t}p^c_{1,2,\mathbf{k}}\Big|_{\mathrm{scatt}} \\ & + (f^{c1}_{\mathbf{k}} - f^{c2}_{\mathbf{k}})\Big[j^c_{2,1}A_{\mathrm{THz}} - \sum_{\mathbf{q}\neq\mathbf{k}} V_{\mathbf{k}-\mathbf{q}}p^c_{1,2,\mathbf{q}}\Big] \\ & + S^{\mathrm{coh}}_{\mathbf{k}}, \end{aligned} \quad (2)$$

where $\tilde{\varepsilon}^c_{l,\mathbf{k}}$ are the renormalized single-particle energies, $f^{c,l}_{\mathbf{k}}$ are the optically excited carrier distributions in the conduction bands, and $V_{\mathbf{q}}$ is the Coulomb matrix element. The term $\frac{\partial}{\partial t}p^c_{1,2,\mathbf{k}}|_{\mathrm{scatt}}$ formally contains all scattering effects and $S^{\mathrm{coh}}_{\mathbf{k}}$ includes the coupling to optically excited interband coherences via the Coulomb interaction. The scattering terms are modeled by a phenomenological dephasing constant γ to match the measured 440 fs decay, i.e., $\frac{\partial}{\partial t}p^c_{1,2,\mathbf{k}}|_{\mathrm{scatt}} \approx -i\gamma p^c_{1,2,\mathbf{k}}$. This approximation is justified since in our case, the intersubband transitions are not affected by excitonic effects due to large experimental linewidths (roughly 3.3 meV). For large time delays of optical pump and THz probe pulses, the optically excited coherences have decayed such that $S^{\mathrm{coh}}_{\mathbf{k}}$ does not contribute.

In our numerical evaluations, we compute the single-particle energies of the quantum-well system using standard $\mathbf{k}\cdot\mathbf{p}$ perturbation theory. For the THz response, we include the first two conduction subbands and the first heavy-hole and light-hole subband [Fig. 1(b)]. As input for the time-dependent fields, we use the experimental THz-pulse shapes of the reference pulse.

The theoretical results are superimposed to the experimental results in Fig. 2. The (red) solid line in Figs. 2(c) and 2(e) represents the absolute value of the computed current density, i.e., the differential transmission for the ps (c) and fs excitation (e). Figure 2(d) separates the two contributions J_{A} (dotted line) and J_{THz} (blue dashed line) to the total current for the case of ps excitation. The solid line in Fig. 2(f) shows the computed absorption spectrum.

In all cases, an excellent experiment-theory agreement is obtained.

As in the measurement, we clearly notice the double peaked Fano-like feature in the transmission spectra, whereas the absorption is only single peaked. In our theory, the origin of the Fano-like feature can be investigated looking at the individual contributions separately. J_A directly reflects the vector potential of the THz probe pulse while J_{THz} consists of the intersubband resonance weighted with the pulse spectrum. The broad feature in the transmission spectrum is a direct consequence of the broad probe pulse. The Fano-like line shape is caused by the phase sensitive superposition of the broad ponderomotive and the sharp intersubband contribution, $|J_{tot}| = |J_A + J_{THz}|$. A further analysis reveals that for frequencies smaller than $\nu_{1,2}$, both contributions partially compensate each other while they interfere constructively for larger frequencies. As for typical Fano situations, this kind of superposition leads to narrowing of the resonance at the low-frequency side and a broadening at the high-frequency side, resulting in the characteristic asymmetric Fano line shape. Since the ponderomotive current leads to a real-valued susceptibility, there is no Fano-like behavior in the THz absorption [Fig. 2(f)].

In order to explain the more pronounced ponderomotive feature in the fs experiment, we had to extend our model beyond the single-quantum-well response. Since the fs pump pulse is spectrally significantly broader than the line width of the 1s exciton resonance (18.2 meV vs 3.3 meV), some frequency components are transmitted through the quantum wells and excite carriers in the substrate. These carriers contribute to J_A but not to J_{THz}, since there are no subbands in bulk material. A quantitative investigation of the interband optical excitation shows that 46% of the pump pulse is transmitted through the quantum wells and absorbed by the substrate. Hence, the total carrier density (in the wells plus substrate) is 1.85 times larger than the density in the quantum wells alone. Since J_A is proportional to the carrier density, we can model the substrate contribution to the THz response simply by enhancing J_A relative to J_{THz} by 1.85. The resulting current density is shown as the red solid line in Fig. 2(e). In the ps experiment, substrate excitations can be neglected since only 1.4% of the pump pulse reaches the substrate.

In summary, we have shown how the emission by the ponderomotive motion of the excited carriers can directly be identified in the linear THz response. Using a microscopic theory for the THz response, the observed Fano-like features in the transmission spectrum can unambiguously be attributed to the phase sensitive superposition of the intersubband resonance and the ponderomotive carrier dynamics. Our results are connected to the typical Fano situation because the system has a sharp discrete intersubband resonance that interferes with a broad continuous contribution, i.e., the ponderomotive current density. However, one of the contributions in our case is nonabsorptive such that we do not observe the Fano resonance in the absorption spectrum but in the differential transmission spectrum only.

The authors from Forschungszentrum Dresden-Rossendorf are grateful to Dr. Stephan Winnerl for critical discussions. The Marburg work is supported by the Quantum Optics in Semiconductors DFG Research Group. The Vienna group is supported by the Austrian FWF.

*daniel.golde@physik.uni-marburg.de

[1] A. Bonvalet *et al.*, Phys. Rev. Lett. **76**, 4392 (1996).
[2] J. N. Heyman, R. Kersting, and K. Unterrainer, Appl. Phys. Lett. **72**, 644 (1998).
[3] R. Kersting *et al.*, Opt. Lett. **25**, 272 (2000).
[4] T. Müller *et al.*, Phys. Rev. B **70**, 155324 (2004).
[5] C. W. Luo *et al.*, Phys. Rev. Lett. **92**, 047402 (2004).
[6] R. H. M. Groeneveld and D. Grischkowsky, J. Opt. Soc. Am. B **11**, 2502 (1994).
[7] J. Cerne *et al.*, Phys. Rev. Lett. **77**, 1131 (1996).
[8] R. Huber *et al.*, Nature (London) **414**, 286 (2001).
[9] R. A. Kaindl *et al.*, Nature (London) **423**, 734 (2003).
[10] I. Galbraith *et al.*, Phys. Rev. B **71**, 073302 (2005).
[11] B. E. Cole *et al.*, Nature (London) **410**, 60 (2001).
[12] S. Leinß *et al.*, Phys. Rev. Lett. **101**, 246401 (2008).
[13] J. F. Dynes *et al.*, Phys. Rev. Lett. **94**, 157403 (2005).
[14] K. B. Nordstrom *et al.*, Phys. Rev. Lett. **81**, 457 (1998).
[15] A. H. Chin, J. M. Bakker, and J. Kono, Phys. Rev. Lett. **85**, 3293 (2000).
[16] J. B. Krieger and G. J. Iafrate, Phys. Rev. B **33**, 5494 (1986).
[17] F. Bloch, Z. Phys. **52**, 555 (1929).
[18] J. R. Danielson *et al.*, Phys. Rev. Lett. **99**, 237401 (2007).
[19] U. Fano, Phys. Rev. **124**, 1866 (1961).
[20] J. Faist *et al.*, Opt. Lett. **21**, 985 (1996).
[21] J. Faist *et al.*, Nature (London) **390**, 589 (1997).
[22] H. Schmidt *et al.*, Appl. Phys. Lett. **70**, 3455 (1997).
[23] H. C. Liu *et al.*, Appl. Phys. Lett. **91**, 131121 (2007).
[24] R. A. Kaindl *et al.*, Opt. Lett. **23**, 861 (1998).
[25] M. Helm, in *Semiconductors and Semimetals*, edited by H. C. Liu and F. Capasso (Academic Press, San Diego, 2000), Vol. 62, Chap. 1.
[26] K. Liu, J. Xu, and X.-C. Zhang, Appl. Phys. Lett. **85**, 863 (2004).
[27] C. Kübler *et al.*, Appl. Phys. Lett. **85**, 3360 (2004).
[28] R. A. Kaindl *et al.*, Phys. Rev. B **63**, 161308(R) (2001).
[29] M. Kira and S. W. Koch, Prog. Quantum Electron. **30**, 155 (2006).
[30] The electrons experience a wiggling motion also in the growth direction due to the tilting of the confinement potential.
[31] H. Haug and S. W. Koch, *Quantum Theory of the Optical and Electronic Properties of Semiconductors* (World Scientific, Singapore, 2009), 5th ed.